# PROCEEDINGS OF SPIE

SPIEDigitalLibrary.org/conference-proceedings-of-spie

Modeling the variation in speed of sound between couplant and tissue improves the spectral accuracy of multispectral optoacoustic tomography

Hong Yang, Dominik Jüstel, Jaya Prakash, Vasilis Ntziachristos

Hong Yang, Dominik Jüstel, Jaya Prakash, Vasilis Ntziachristos, "Modeling the variation in speed of sound between couplant and tissue improves the spectral accuracy of multispectral optoacoustic tomography," Proc. SPIE 10890, Label-free Biomedical Imaging and Sensing (LBIS) 2019, 1089027 (4 March 2019); doi: 10.1117/12.2506425



Event: SPIE BiOS, 2019, San Francisco, California, United States

# Modeling the variation in speed of sound between couplant and tissue improves the spectral accuracy of multispectral optoacoustic tomography

Hong Yang<sup>1,2</sup>, Dominik Jüstel<sup>1,2</sup>, Jaya Prakash<sup>1,2</sup>, Vasilis Ntziachristos<sup>1,2,\*</sup>

<sup>1</sup>Institute for Biological and Medical Imaging, Helmholtz Zentrum Munich, Neuherberg, Germany. <sup>2</sup>Chair of Biological Imaging, Technical University of Munich, Munich, Germany

Corresponding author: Vasilis Ntziachristos, Ph.D., Helmholtz Zentrum München, Ingolstädter Landstrasse 1, D-85764 Neuherberg, Germany. Tel: +49 89 3187 3852. Email: v.ntziachristos@tum.de

#### **ABSTRACT**

Even though the speed of sound (SoS) is non-homogeneous in biological tissue, most reconstruction algorithms for optoacoustic imaging neglect its variation. In addition, when heavy water is used as coupling medium to enable imaging of certain biological chromophores such as lipids and proteins, the SoS also differs significantly between couplant and tissue.

While the assumption of uniform SoS is known to introduce visible deformations of features in single-wavelength optoacoustic images, the spectral error introduced by the assumption of uniform SoS is not fully understood. In this work, we provide an in-depth spectral analysis of multi-spectral optoacoustic imaging artifacts that result from the assumption of uniform SoS in situations where SoS changes substantially.

We propose a dual-SoS model to incorporate the SoS variation between the couplant and the sample. Tissue-mimicking phantom experiments and *in vivo* measurements show that uniform SoS reconstruction causes spectral smearing, which dual-SoS modeling can largely eliminate. Due to this increased spectral accuracy, the method has the potential to improve clinical studies that rely on quantitative optoacoustic imaging of biomolecules like hemoglobin or lipids.

**Keywords**: photoacoustic, multi-spectral optoacoustic imaging, image reconstruction, spectral smearing, handheld system.

#### 1. INTRODUCTION

Optoacoustic (photoacoustic) tomography involves shining biological samples with light in the near-infrared (NIR) regime (700-1050 nm) and collecting the generated acoustic signals using tomographic detection geometry <sup>[1]</sup>. The acquired tomographic signals are reconstructed based on the time of flight of acoustic waves. The time of flight depends on the traversed distance and the Speed of Sound (SoS) distribution in the Field of View (FOV). During optoacoustic reconstruction, the imaging medium is normally assumed to be acoustically homogeneous and SoS to be therefore invariant, enabling the derivation of a closed-form solution to the acoustic wave equation <sup>[2]</sup>. However, this assumption leads to visible artifacts on the image when the variation of the SoS in the FOV is around or larger than 10% <sup>[3]</sup>. In most cases, 10% SoS variation can be easily met, such as the SoS variation between different tissue types or between couplant and sample, especially when heavy water is used as coupling medium <sup>[4]</sup>. For imaging biological chromophores like lipids and proteins <sup>[5]</sup>, heavy water is essential in these cases since light absorption is much lower in heavy water than in water at wavelengths >900 nm <sup>[6]</sup>. For example, an optoacoustic imaging set-up with heavy water as coupling medium has successfully imaged fatty tumors and showed the potential of optoacoustic tomography in the diagnosis and evaluation of subcutaneous soft-tissue masses <sup>[5]</sup>. Heavy water is also needed as coupling medium when simultaneously

Label-free Biomedical Imaging and Sensing (LBIS) 2019, edited by Natan T. Shaked, Oliver Hayden, Proc. of SPIE Vol. 10890, 1089027 · © 2019 SPIE CCC code: 1605-7422/19/\$18 · doi: 10.1117/12.2506425

imaging lipid and hemoglobin while also determining oxygen saturation, which is required for many cardiovascular and oncological applications [7, 8].

The reconstruction artifacts induced by uniform SoS model have attracted increasing attention in recent years. Prior work has shown that uniform SoS can introduce localization errors, reconstruct absorbers with inaccurate dimensions, and decrease the maximal resolution of the recovered image <sup>[6]</sup>. Other studies have described additional artifacts such as smearing and deformation of absorbers due to the assumption of constant SoS, and these artifacts are difficult to reduce using post-processing schemes <sup>[9, 10]</sup>. All these studies have focused on image artifacts in single-wavelength optoacoustic data. Much less understood is the impact of uniform SoS reconstruction on the spectra of chromophores in multi-spectral optoacoustic data. It is likely that the impact of such artifacts on multi-spectral optoacoustic imaging is underestimated, and that they can hinder quantitative analysis of reconstructed spectral information <sup>[11]</sup>, such as the analysis of endogenous chromophores such as lipids and proteins <sup>[12]</sup>.

Therefore, in this study we analyzed the spectral artifacts of multi-spectral optoacoustic imaging induced by assuming uniform SoS. The analysis is based on the multi-spectral optoacoustic images of a phantom and human tissue *in vivo*, allowing us to develop and evaluate a dual-SoS model that can assign different SoS values in couplant and the sample. Our model extends the algebraic reconstruction technique (ART) type model-based reconstruction using interpolated-matrix-model inversion (IMMI) [13] and angular discretization strategy [14] to include dual SoS.

#### 2. MATERIAL AND METHODS

#### 2.1 Reconstruction using uniform/single SoS

For optoacoustic imaging, when a short nanosecond laser pulse is used as the light source, the propagation of the acoustic wave  $p(\mathbf{r},t)$  at spatial position  $\mathbf{r}$  and time instant t can be described as [14],

$$\frac{\partial^2 p(\mathbf{r},t)}{\partial t^2} - c^2 \nabla^2 p(\mathbf{r},t) = \Gamma H(\mathbf{r}) \frac{\partial \delta(t)}{\partial t}$$
 (1)

where c is the SoS in the FOV,  $\Gamma$  is Grueneisen parameter,  $\delta(t)$  presents the laser pulse and  $H(\mathbf{r})$  is the absorbed energy per unit volume. Based on Eq. (1), the pressure distribution in a 2D acoustically homogeneous space (uniform/single SoS) can be written as,

$$p(\mathbf{r},t) = \frac{\Gamma}{4\pi c} \int_{L(t)} \frac{H(\mathbf{r}')}{|\mathbf{r} - \mathbf{r}'|} dL(t)$$
 (2)

With multiple transducer positions and time instants, a system of linear equations can be formulated by discretizing the integral and expressed in a matrix form as,

$$\mathbf{P} = \mathbf{A}_{single} \mathbf{H} \tag{3}$$

where  $\mathbf{A}_{single}$  is the model matrix with uniform SoS. With limited-view tomographic handheld set-up, the inversion of last equation is conveniently achieved with regularization,

$$\mathbf{H}_{sol} = \underset{\mathbf{u}}{\operatorname{arg\,min}} \left\| \mathbf{P}_{m} - \mathbf{A}_{single} \mathbf{H} \right\|^{2} + \lambda \left\| \mathbf{L} \mathbf{H} \right\|^{2}$$
(4)

where  $P_m$  is the measured pressure signals with ultrasound transducers,  $\lambda$  is the regularization parameter and L is a 2D Laplace operator.

#### 2.2 Reconstruction using dual SoS

When the SoS difference between couplant and sample is considered (dual-SoS), Eq. (2) is rewritten as:

$$p(\mathbf{r},t) = \frac{\Gamma}{4\pi c_1} \int_{L(t)} \frac{H(\mathbf{r}')}{|\mathbf{r} - \mathbf{r}'|} dL_1(t) + \frac{\Gamma}{4\pi c_2} \int_{L_2(t)} \frac{H(\mathbf{r}')}{|\mathbf{r} - \mathbf{r}'|} dL_2(t)$$
(5)

where  $L_1(t) \in |\mathbf{r} - \mathbf{r}'| = c_1 t$ ,  $L_2(t) \in |\mathbf{r} - \mathbf{r}'| = c_2 t$ ,  $c_1$  and  $c_2$  are the SoS in couplant, e.g. heavy water and tissue sample in this study, respectively. We split the integral into two regions, assuming that wave equation is linear with respect to SoS variation. With multiple detection angles and discretization, last equation can be expressed as,

$$\mathbf{P} = \mathbf{A}_{dual} \mathbf{H} \tag{6}$$

where  $A_{dual}$  is the model matrix with dual SoS. The inversion of Eq. 6 can be achieved as,

$$\mathbf{H}_{sol} = \underset{\mathbf{H}}{\operatorname{arg}} \min_{\mathbf{H}} \|\mathbf{P}_{m} - \mathbf{A}_{dual} \mathbf{H}\|^{2} + \lambda \|\mathbf{L}\mathbf{H}\|^{2}$$
(7)

The computational complexity of Eq. (2) and Eq. (5) is the same, i.e. the dual-SoS reconstruction can contribute to more accurate results than uniform SoS reconstruction without increasing computational cost.

In order to compare the spectral performance between the two different reconstruction schemes (single SoS and dual-SoS), spectral similarity  $S(\mathbf{I}_i, \mu_a)$  between the normalized optoacoustic intensity spectrum in each pixel  $\mathbf{I}_i$  and the normalized absorption spectrum of target chromophore  $\mu_a$  is calculated [15]:

$$S(\mathbf{I}_{i}, \mu_{a}) = -\|\mathbf{I}_{i}(\lambda) - \mu_{a}(\lambda)\|_{2}^{2}$$
(8)

#### 2.3 Imaging set-up and operation

Measurements from the clinical handheld multi-spectral optoacoustic tomography system (Acuity 256; iThera Medical GmbH, Munich, Germany) [16, 17] was used to evaluate the proposed methods. The dual-SoS model was designed based on the geometry of handheld probe shown in Fig.1. Fig. 1a shows the probe of Acuity system and this probe has 256 cylindrically focused transducer elements (of 4 MHz central frequency). Fig. 1b schematically shows the geometric structure of detector array, i.e. 60 mm focal length and 145°angular coverage. The sample is illuminated with a nanosecond pulse laser (10 ns and maximum energy of 25 *mJ*) at a 25 Hz repetition rate and 28 wavelengths are scanned from 700 nm to 970 nm with 10 nm interval. In this set-up, heavy water is used as the coupling medium (embedded in the probe) to minimize the light energy loss due to water absorption to enable imaging of all chromophores whose spectral signature is between 700 nm-1000 nm. Importantly the SoS difference between heavy water and tissue is large (around 1400m/s in heavy water and 1560m/s in tissue [4]), and the large SoS variation will introduce obvious spectral error when uniform SoS is considered.

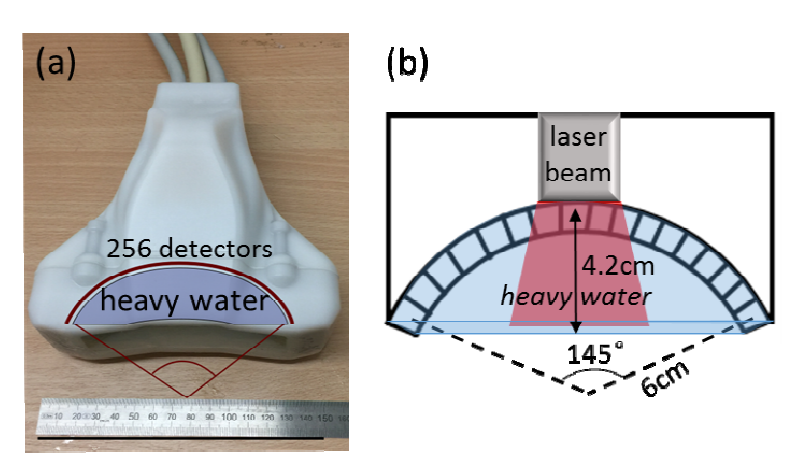


Fig. 1 Handheld MSOT Probe (Acuity). (a) Photograph of the probe. (b) Schematic diagram of the probe showing the geometry of detector array and a built-in cavity filled with heavy water as coupling medium.

# 2.4 Experimental measurements -- phantoms and human tissue

The spectral error introduced by uniform SoS model and the efficiency of dual-SoS reconstruction were evaluated using a cylindrical Agar phantom with three plastic tube insertions. The background of the phantom is made with a mixture of

agar, distilled water and intralipid and the tubes contain indocyanine green (ICG,  $\mu_a(750nm) = 2.1 \,\mathrm{cm}^{-1}$ ), Alexafluor750 (AF750,  $\mu_a(750nm) = 4.2 \,\mathrm{cm}^{-1}$ ) and Indian ink ( $\mu_a(750nm) = 3.9 \,\mathrm{cm}^{-1}$ ) solution, respectively. Therefore SoS inside the phantom is close to the SoS in water, i.e. approximately 1500m/s. The absorption spectra of ICG, AF750 and ink were measured with a spectrometer before imaging experiments. Further the spectral accuracy of the proposed reconstruction schemes were studied with *in vivo* measurements, to this end the forearm of a healthy volunteer was imaged.

# 3. RESULTS

Fig. 2 evaluates and compares reconstructions of the phantom carried out assuming single SoS (Eq. 4) or dual SoS (Eq. 7). Fig. 2a shows anatomical deformation with assumption of single SoS, consistent with previous studies <sup>[3, 9]</sup>. Fig 2b shows that using dual-SoS reconstruction reduces the deformation, allowing the signal to converge to a circular structure. To compare the two SoS approaches in greater detail, Fig. 2c plots the mean intensities of a small region inside the middle tube (indicated as P1) as a function of wavelengths, while Fig. 2d plots the mean intensities outside the tube (indicated as P2). As the tube in the middle contains AF750 solution, the spectrum of P1 should be similar to the absorption spectrum of AF750 measured with spectrometer labeled as 'AF750' in Fig. 2c and 2d. In contrast, the spectrum of P2 should not bear any resemblance to the AF750 absorption spectrum, since P2 is a background region containing primarily water, which absorbs negligibly below 900 nm. Fig. 2c shows that reconstruction assuming either uniform or dual-SoS recovers the AF750 spectrum in P1. Fig. 2d indicates that only dual-SoS reconstruction accurately gives a noisy spectrum at P2, whereas single SoS reconstruction shows a spectral signature similar to AF750. In other words, assuming uniform SoS causes "spectral smearing" in which spectral information of an absorber smears over neighboring regions.

Fig. 2e shows spatial analysis of this spectral smearing by quantifying the similarity between the spectrum observed in Fig. 2a and the absorption spectrum of AF750: spectral similarity is greatest in the middle tube containing AF750, and the smearing extends to the very bottom of the image to form two obvious smearing 'tails' (dashed ellipses in Fig. 2e). Fig. 2f shows that with dual-SoS reconstruction, spectral similarity values are highest only in the middle tube, and smearing 'tails' are largely eliminated. Comparing Fig. 2e and 2f indicates that single SoS reconstruction can cause extensive spectral smearing even when it is less obvious in the single-wavelength images, and that this smearing can be drastically reduced by modeling the SoS variation between couplant and sample.

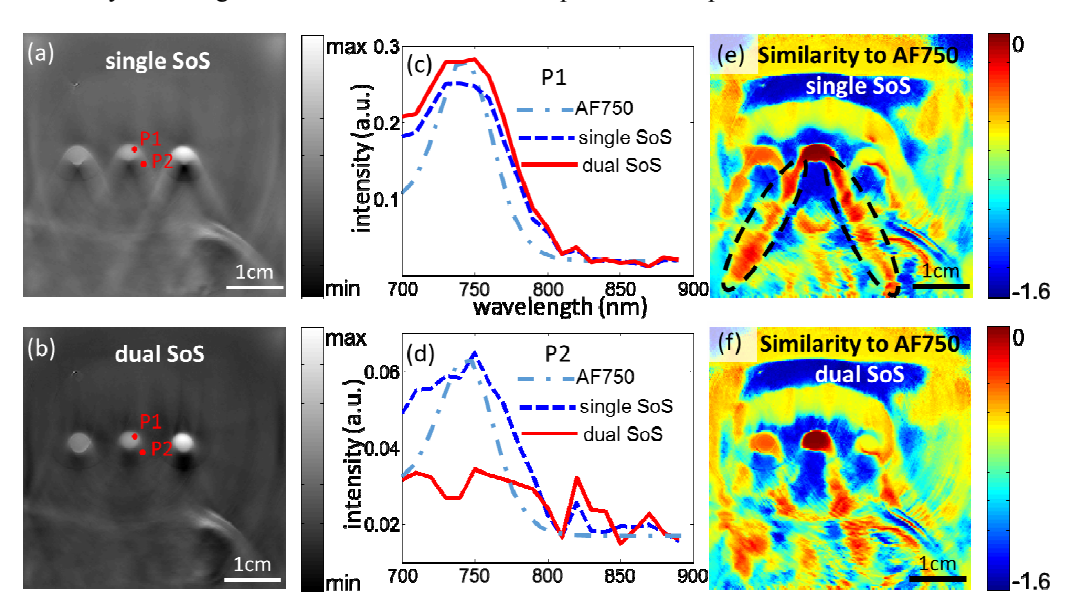


Fig. 2 Reconstruction of a phantom with uniform SoS and dual-SoS model. (a) Reconstruction of the phantom with uniform SoS. (b) Reconstruction of the phantom with dual SoS. (c) Spectra of P1 in (a) and (b). (d) Spectra of P2 in (a) and (b). (e) Spectral similarity map of the reconstructed dataset with uniform SoS to the spectrum of Alexaflour750 from spectrometer. (f) Spectral similarity map of the reconstructed dataset with dual-SoS to the spectrum of Alexaflour750. Red dots indicate the area (~ 15 pixels) whose spectra are shown in panels (c) and (d). Scale bars are 1 cm.

Furthermore, we extended this comparison of single and dual-SoS reconstruction to biological samples. Fig. 3 compares the two reconstructions of a region of forearm in a healthy volunteer. Fig. 3a reveals substantial deformation of blood vessel shape due to the assumption of uniform SoS, whereas Fig. 3b shows the expected circular shape when dual-SoS model is used. In order to quantify spectral smearing just as we did for the phantom dataset, we had to modify our procedure to take into account the more heterogeneous background intensities of the tissue as well as the fact that we had no prior information about the exact distribution of chromophores within imaged tissue. As the subcutaneous fat layer is easily identifiable, we analyzed the similarity between the reconstructed spectra of pixels in the observed reconstructions and the reference absorption spectrum of lipid (the major component of fat) labeled as 'lipid' in Fig. 3c and 3d. Fig. 3c and 3d compare the reconstructed spectra in an area inside the subcutaneous fat layer (marked as P1) and in an area below the fat layer (P2). Fig. 3c and 3d show that assuming single SoS leads to a lipid-like spectrum in both P1 and P2, whereas applying dual-SoS more accurately reconstructs the spectrum in P2.

Fig. 3e and 3f show spatial analysis of the similarity of reconstructed spectra of pixels in Fig. 3a and 3b with the absorption spectrum of fat. The red color indicates high similarity to the fat spectrum, which should be observed only in the fat layer. The region enclosed within a black dashed ellipse in Fig. 3e shows that the spectrum of the blood vessel smears into the surrounding fat layer and creates a sharp gap (indicated with black arrow) in the similarity map. Meanwhile, dual-SoS reconstruction recovers a spatially continuous fat distribution in the subcutaneous fat layer, which is biologically more reasonable.

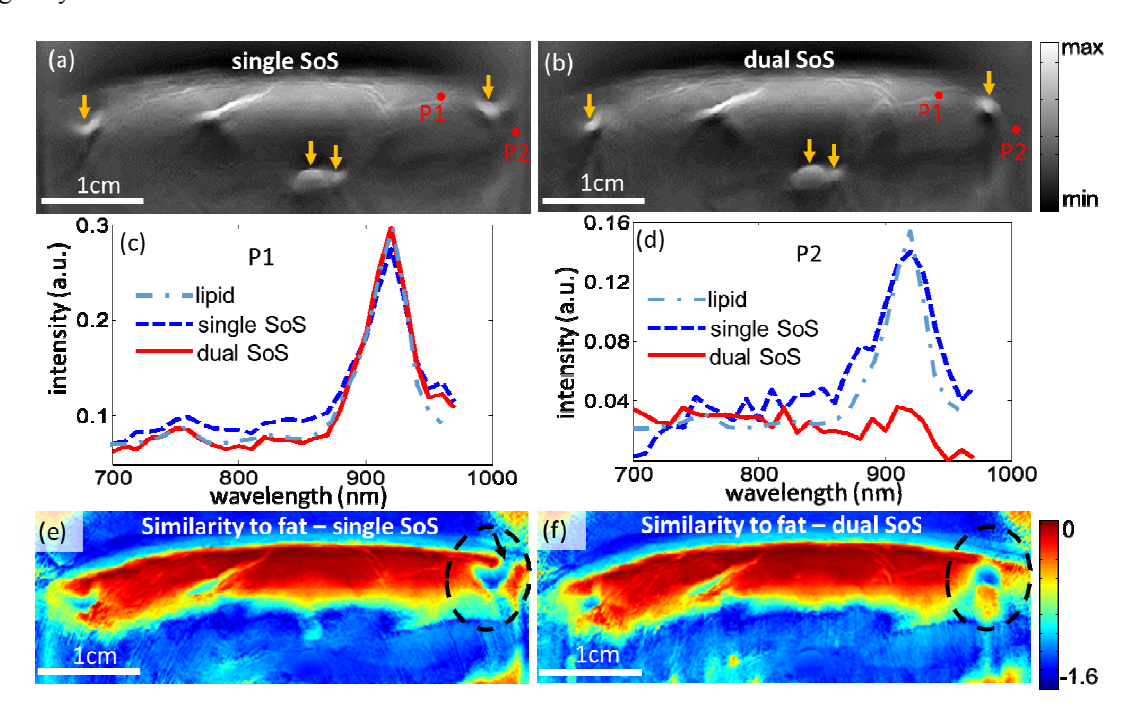


Fig. 3 Comparison of image reconstruction of human forearm assuming uniform SoS or dual SoS. (a) Reconstruction assuming uniform SoS at 930 nm. (b) Reconstruction assuming dual-SoS at 930 nm. (c) Reconstructed spectra at P1 in panels (a) and (b). (d) Reconstructed spectra at P2 in panels (a) and (b). (e) Spectral similarity between the spectrum at each pixel in panel (a) and the spectrum of fat from spectrometer. (f) Similarity between the spectrum at each pixel in panel (b) and the spectrum of lipid from spectrometer. Red dots indicate the area (~ 15 pixels) whose spectra are shown in panels (c) and (d), and yellow arrows indicate blood vessels. Scale bars are 1 cm.

### 4. DISCUSSION

Here we provide the spectral analysis of multi-spectral optoacoustic imaging artifacts induced by assuming uniform SoS in situations where the SoS changes substantially, such as when the coupling medium is heavy water. This spectral analysis allowed us to develop a reconstruction algorithm that takes into account dual SoS, and this algorithm more faithfully reproduced the absorption spectra of chromophores in a phantom and tissue *in vivo*. This approach may serve as a basis for more accurate unmixing of optoacoustic signals from a range of chromophores, including oxy- and deoxy-

hemoglobin, fat, and water. In this way, dual-SoS model may improve the unique ability of multi-spectral optoacoustic imaging to simultaneously visualize numerous parameters of health and disease non-invasively in real time.

Previous studies examined artifacts induced by invariant SoS in single-wavelength optoacoustic imaging, and they demonstrated visual smearing of key features in the reconstructed image. Here we demonstrate the spectral equivalent, which we term "spectral smearing", when uniform SoS is assumed during reconstruction of multi-wavelength optoacoustic images. We show that this assumption can lead to substantial spectral distortion even when visual distortion is less obvious in reconstructed images; such spectral smearing can substantially affect the accuracy of the unmixing. This results in inaccurate quantitation of functional tissue parameters and distribution of chromophores, which is precisely where multi-spectral optoacoustic imaging can offer a high-resolution, non-invasive advantage over other imaging methods.

The dual-SoS model developed in this study can be easily adapted to other coupling media, such as water and ultrasound gel, without increasing computational cost. This model may be useful for handling SoS variation not only between sample and coupling medium, but also between different tissues inside the sample, such as fat and muscle. An extension from dual-SoS model to spatially variant SoS model in the whole FOV should improve spectral unmixing results and subsequent quantitation of molecules in tissues. This should be tested directly in future controlled experiments.

In conclusion, we studied the influence of uniform SoS modeling on spectral accuracy and the benefits of using a dual-SoS model to account for the SoS variation between couplant and tissue sample. The dual-SoS model was developed by employing two SoS in the imaged region specifically focused towards imaging lipids and biomolecules. The spectral smearing introduced by uniform SoS reconstruction was quantified and the dual-SoS reconstruction was demonstrated to be able to correct the spectral smearing and lead to more accurate spectral information. As spectral accuracy is the foundation of molecular optoacoutic imaging, dual-SoS reconstruction should be applied in the future to avoid spectral smearing and enable accurate unmixing of different chromophores like oxyhemoglobin, deoxyhemoglobin, and lipids.

#### 5. ACKNOWLEDGEMENT

H. Yang acknowledges the support of the CSC Fellowship (201506960010), and the authors acknowledge Chapin Rodriguez for editing the paper.

#### 6. REFERENCE

- [1] A. Dima, N. C. Burton, and V. Ntziachristos, "Multispectral optoacoustic tomography at 64, 128, and 256 channels," Journal of biomedical optics, 19(3), 036021-036021 (2014).
- [2] M. Xu, and L. V. Wang, "Universal back-projection algorithm for photoacoustic computed tomography," Physical Review E, 71(1), 016706 (2005).
- [3] X. L. Deán-Ben, V. Ntziachristos, and D. Razansky, "Effects of small variations of speed of sound in optoacoustic tomographic imaging," Medical physics, 41(7), (2014).
- [4] H. Azhari, "Typical acoustic properties of tissues," Basics of Biomedical Ultrasound for Engineers, 313-314 (2010).
- [5] A. Buehler, G. Diot, T. Volz *et al.*, "Imaging of fatty tumors: appearance of subcutaneous lipomas in optoacoustic images," Journal of Biophotonics, (2017).
- J. Bayly, V. Kartha, and W. Stevens, "The absorption spectra of liquid phase H2O, HDO and D2O from 0· 7 μm to 10 μm," Infrared Physics, 3(4), 211-222 (1963).
- [7] A. E. Zavodni, B. A. Wasserman, R. L. McClelland *et al.*, "Carotid artery plaque morphology and composition in relation to incident cardiovascular events: the Multi-Ethnic Study of Atherosclerosis (MESA)," Radiology, 271(2), 381-389 (2014).
- [8] J. Wang, B. W. Pogue, S. Jiang *et al.*, "Near-infrared tomography of breast cancer hemoglobin, water, lipid, and scattering using combined frequency domain and cw measurement," Optics letters, 35(1), 82-84 (2010).
- [9] J. Jose, R. G. Willemink, W. Steenbergen *et al.*, "Speed-of-sound compensated photoacoustic tomography for accurate imaging," Medical physics, 39(12), 7262-7271 (2012).
- [10] L. Li, L. Zhu, C. Ma *et al.*, "Single-impulse panoramic photoacoustic computed tomography of small-animal whole-body dynamics at high spatiotemporal resolution," Nature Biomedical Engineering, 1(5), Art. No. 0071 (2017).

- [11] V. Ntziachristos, and D. Razansky, "Molecular imaging by means of multispectral optoacoustic tomography (MSOT)," Chemical reviews, 110(5), 2783-2794 (2010).
- [12] D. Razansky, J. Baeten, and V. Ntziachristos, "Sensitivity of molecular target detection by multispectral optoacoustic tomography (MSOT)," Medical physics, 36(3), 939-945 (2009).
- [13] A. Rosenthal, D. Razansky, and V. Ntziachristos, "Fast semi-analytical model-based acoustic inversion for quantitative optoacoustic tomography," IEEE transactions on medical imaging, 29(6), 1275-1285 (2010).
- [14] X. L. Deán-Ben, V. Ntziachristos, and D. Razansky, "Acceleration of optoacoustic model-based reconstruction using angular image discretization," IEEE Transactions on medical imaging, 31(5), 1154-1162 (2012).
- [15] B. J. Frey, and D. Dueck, "Clustering by passing messages between data points," science, 315(5814), 972-976 (2007).
- [16] A. Buehler, M. Kacprowicz, A. Taruttis *et al.*, "Real-time handheld multispectral optoacoustic imaging," Optics letters, 38(9), 1404-1406 (2013).
- [17] A. Dima, and V. Ntziachristos, "In-vivo handheld optoacoustic tomography of the human thyroid," Photoacoustics, 4(2), 65-69 (2016).